Quantifying cellular traction forces in three dimensions

Stacey A. Maskarinec[a,1], Christian Franck[b,1,2], David A. Tirrell[a], and Guruswami Ravichandran[c]

[a]Division of Chemistry and Chemical Engineering, California Institute of Technology, 1200 East California Boulevard, MC 210-41, Pasadena, CA 91125; [b]Division of Engineering, Brown University, 182 Hope Street, Box D, Providence, RI 02912; and [c]Division of Engineering and Applied Science, California Institute of Technology, 1200 East California Boulevard, MC 105-50, Pasadena, CA 91125

Edited by Steven G. Boxer, Stanford University, Stanford, CA, and approved November 2, 2009 (received for review April 27, 2009)

Cells engage in mechanical force exchange with their extracellular environment through tension generated by the cytoskeleton. A method combining laser scanning confocal microscopy (LSCM) and digital volume correlation (DVC) enables tracking and quantification of cell-mediated deformation of the extracellular matrix in all three spatial dimensions. Time-lapse confocal imaging of migrating 3T3 fibroblasts on fibronectin (FN)-modified polyacrylamide gels of varying thickness reveals significant in-plane (x, y) and normal (z) displacements, and illustrates the extent to which cells, even in nominally two-dimensional (2-D) environments, explore their surroundings in all three dimensions. The magnitudes of the measured displacements are independent of the elastic moduli of the gels. Analysis of the normal displacement profiles suggests that normal forces play important roles even in 2-D cell migration.

digital volume correlation | laser scanning confocal microscopy | three-dimensional

The measurement of cellular traction forces has been of increasing interest since the discovery that the mechanical properties of the cellular microenvironment can direct many important cellular processes including spreading, migration, and differentiation (1–4). It is now widely accepted that mechanical properties must be considered along with chemical signals if we are to understand how cells integrate environmental cues to modulate their behavior (5–8). The correlation between cell-induced deformations in materials and biochemical signaling and regulation, particularly focal adhesion formation and clustering, has been investigated through the use of a variety of techniques including surface wrinkling, displacement-tracking using traction force microscopy (TFM), and bending of pillar arrays (9–15). These methods have yielded substantial insight into cellular behavior, but are inherently restricted to two-dimensional (2-D) analysis and interpretation of cell-matrix interactions. Furthermore, these approaches calculate stresses by comparing images before and after cell detachment (10), thus providing only snapshots of cell behavior rather than dynamic analyses of the processes by which cells explore their microenvironments.

In this report, we demonstrate the capability to dynamically track and quantify cellular traction forces in three dimensions (3-D). Mechanical interactions between 3T3 fibroblasts and FN-modified polyacrylamide gels are quantified dynamically by computing the displacement and traction fields generated by motile cells. Use of a recently developed digital volume correlation (DVC) method (16) allows 3-D displacements and traction fields to be determined directly from volumetric confocal image stacks, and obviates the need for complex inverse formulations (10). The method has a temporal resolution that permits confocal imaging over time scales relevant for the migration of anchorage dependent cells, such as endothelial cells and fibroblasts (17).

The 3-D character of this approach relies on the use of laser scanning confocal microscopy (LSCM), which has the distinct advantage over conventional microscopic imaging in that it provides positional information along the z axis, i.e., in the direction normal to the plane of the sample (18). A schematic of the experimental setup is shown in Fig. 1*A*. The range of gel thicknesses investigated was between 20 and 100 μm, and the height contribution of the covalently attached FN layer measured by confocal scanning was <1 μm. Samples were produced with two different cross-link densities to achieve physiologically relevant values of the elastic modulus [E, 0.82 ($\pm$ 0.23) kPa and 9.64 ($\pm$ 1.12) kPa] (see Figs. S1–S3) (19). Red fluorescent microspheres (0.5 μm in diameter) were embedded and tracked during gel formation to enable calculation of cell-generated deformations using DVC. Simultaneous visualization of the red fluorescent markers and the cell was accomplished by allocating separate lasers and filters along with the use of a 3T3 fibroblast cell line transfected with a vector encoding a green fluorescent protein (GFP)-actin fusion construct. Cells were deposited on the surfaces of the FN-modified samples and incubated overnight to ensure attachment before imaging. Isolated cells were imaged every 35 min for up to 24 h within a typical field of view of $150 \times 150 \times 150$ μm^3. Fig. 1*B* shows a cross-sectional view of a typical confocal stack. Imaging of isolated cells (at a distance of $>$80–100 μm from other cells) ensures that neighboring cells do not contribute to the measured displacements.

As the cell explores the substrate and probes its resistance to deformation, displacements are determined by comparing successive stacks. Most importantly, the DVC method can map such displacements in all three dimensions by comparing uniquely defined cubic subsets of fluorescent particles within confocal stacks that are obtained sequentially (16). This technique can detect both translational and rotational changes, and is valid for large deformations. The technique can resolve displacement changes greater than or equal to 0.12 μm.

Results

3-D Displacement Profiles of Migrating Cells. Detection of both normal and in-plane displacements allows a more complete analysis of cellular forces than does consideration of only in-plane (2-D) displacements (10). Fig. 2 shows the extent of cell-induced deformation as a function of depth within each substrate, and shows clearly that the normal (z) displacement can be comparable to, or greater than, the in-plane displacement. In the images in Fig. 2*A*, a slice along the long axis of the cell is shown, and the cell has been rendered in 3-D, and superimposed to correlate its position with the observed displacements. The colored displacement contours show that larger displacements are concentrated near the top surface of the gel, and that these displacements decay from the top surface through the depth. Comparing the displacement patterns on gels of varying thicknesses, we find that displacements are more localized

Author contributions: S.A.M., C.F., D.A.T., and G.R. designed research; S.A.M. and C.F. performed research; S.A.M. and C.F. contributed new reagents/analytic tools; S.A.M., C.F., D.A.T., and G.R. analyzed data; and S.A.M., C.F., D.A.T., and G.R. wrote the paper.

The authors declare no conflict of interest.

This article is a PNAS Direct Submission.

[1]S.A.M. and C.F. contributed equally to this work.

[2]To whom correspondence should be addressed. E-mail: franck@brown.edu.

This article contains supporting information online at www.pnas.org/cgi/content/full/0904565106/DCSupplemental.

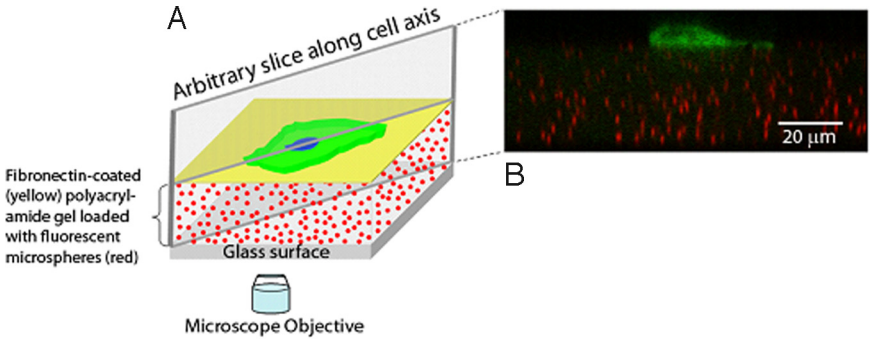

Fig. 1. Confocal imaging of migrating fibroblasts on FN-modified polyacrylamide gels. (*A*) Schematic of a representative gel sample with microscope objective. 3-D confocal image stacks are acquired every 35 min through an inverted microscope that captures the emission from both the fluorescent microspheres (red) and GFP-transfected cells (green). The 35-min time interval was chosen for investigating fibroblast migration patterns given measured migration speeds of approximately 8 μm/h, as well as to minimize phototoxic cell death that was observed at shorter time intervals (see *Materials and Methods*). (*B*) Cross-sectional view of a typical confocal image stack. Cells migrate on the surface of the FN-modified polyacrylamide gel, and the corresponding displacements in the underlying gel are monitored. The red fluorescent microspheres are visible within the gel.

near the cell body on thinner samples (20 μm), and decay more gradually in thicker samples (80 μm). The decay profiles of the magnitude of individual displacement components as well as the total displacements for substrates of varying thicknesses are displayed as line plots in Fig. 2*B*. The total displacement is defined as a vector summation of all three individual displacement component vectors. All plots were generated by selecting one position along the thickness cross-section of the sample near the leading edge of the migrating cell. This position corresponds to the region of maximum deformation at a given time point. Displacement decays are also notable in the x–y displacements, as a function of distance from the cell, and in some cases, drop off more steeply than the z-component. The total displacement profile at a given time point and slice location can be dominated by either in-plane or normal displacements, demonstrating how force-mediated deformations fluctuate during cell movement. Analysis of the ratios of the magnitudes of the individual components of the 3-D displacement vector to the magnitude of the vector itself showed similar values for all three components ($\bar{x} = 0.58 \pm 0.29, \bar{y} = 0.43 \pm 0.23, \bar{z} = 0.50 \pm 0.32$, for $n = 38$ samples), further demonstrating the importance of measuring displacements in all three dimensions.

It is worth noting that deformation of the substrate can be detected at substantial depths below the top surface of each sample, and that this effect can be especially important for thin gels. For example, the fact that measurable displacements extend throughout more than half the thickness of the 20-μm sample, illustrates the importance of considering film thickness in designing experiments to monitor cellular response. In particular, if the substrate thickness is comparable to the extent of the deformation field, a cell seeded on a soft substrate that is bonded to a substantially stiffer support (e.g., glass), may be able to sense the mechanical constraint of the underlying plate. For the samples shown in Fig. 2, the maximum depth at which the cell-induced displacement was detectable (i.e., >0.12 μm) decreased from 67 to 23% of the sample thickness as the gel thickness increased from 20 to 80 μm.

Time Evolution of Cell-Induced Displacement and Traction Fields. Comparing series of confocal stacks affords insight into the time evolution of the displacement and traction profiles produced during cell migration. A planar slice through the top surface of the sample shows how the pattern of displacements changes as a cell moves along the substrate surface (Fig. 3). The set of images in Fig. 3*A* represents 3-D data collapsed into 2-D images, and four successive images of this type are displayed for a 140-min time course of cell migration. The middle panel of parallel images (Fig. 3*B*) shows the total displacements (3-D) of the surface plane as colored contours, while the vectors indicate only in-plane (2-D) displacements. These displacements are then transformed into traction forces in the last panel of complementary images (Fig. 3*C*) using the experimentally determined displacement field and material properties (see *SI Text* and Fig. S4).

A polarized cell extending processes in the form of a leading edge generates localized, contractile stresses that change as it propels itself forward (Fig. 3*C*, 35–70 min). Stresses near the rear of the cell are also observed during migration and have been shown in previous studies to correspond to focal complexes that transmit significant cellular forces (20). Notable forces detected near the rear of the cell during migration in this study may explain previously reported observations, which demonstrated that on surfaces of high and intermediate adhesiveness, cells can become so tightly bound to the substrate that a portion of their trailing edge can be fractured during migration, leaving behind adhesion receptors (e.g., integrins) on the surface (21, 22). A similar range of displacement values observed on samples of varying mechanical properties suggests that under typical culturing conditions, cells maintain relatively constant levels of displacement (independent of modulus) within the range of material properties considered here (*SI Text*). In accordance with previous studies, the calculated forces on more rigid samples are greater than those on softer ones (23). It is important to note that the magnitudes of the forces determined here lie within the range reported for fibroblasts (10, 15), and that these measurements only present the distribution of cellular forces that occur during movement and thus cannot be directly compared to a total detachment force.

Confirmation of the cellular origins of the measured displacements was accomplished by replicating time-lapse experiments followed by treatment with blebbistatin. Addition of this myosin-II-specific blocker (24) resulted in a gradual inhibition of cell-generated displacements, showing that the localized matrix deformations observed were caused by contraction of actin bundles by myosin-II activity (Fig. S5).

At certain time points (e.g., Fig. 3*C*: 105–140 min) significant displacements are measurable beneath the cell body near the nucleus, suggesting that a large portion of the cell's contact area participates in force exchange with the substrate. Examination of the contribution of each force component during cell migration showed notable in-plane forces on the ventral surface of the cell that potentially indicate frictional forces. Further experiments will be needed to define more clearly the cellular origins of these displacements.

Push–Pull Behavior Observed in Normal Displacement Profile of Migrating Cells. In many instances, a cell can be seen pulling the matrix near its trailing edge while simultaneously pushing a

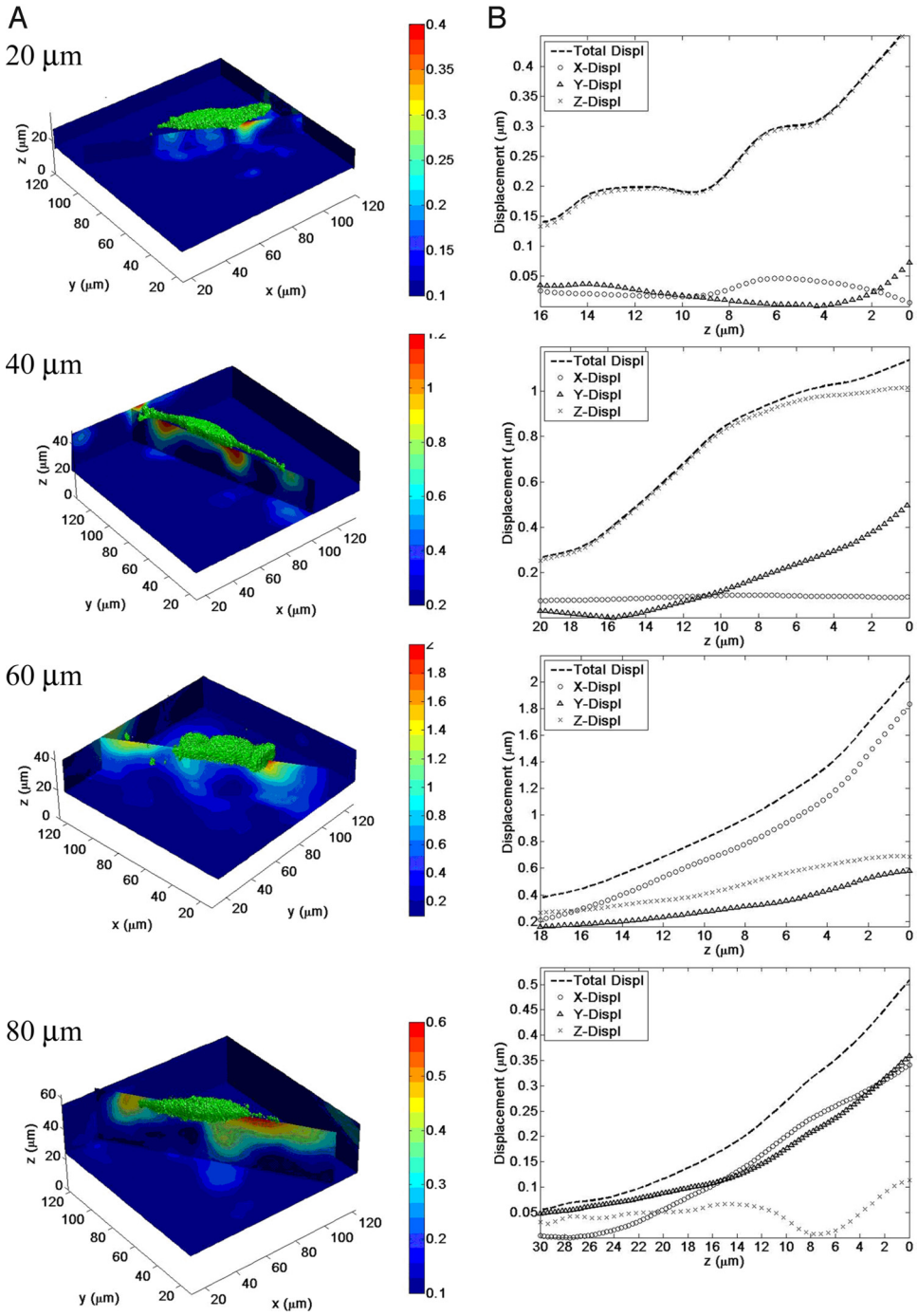

Fig. 2. Displacement contour slices along the long axis of the cell and corresponding displacement line plots as a function of depth for samples of varying heights. (*A*) Slices of displacement contours underneath migrating cells show significant deformation in the normal direction that decays along the thickness of the sample. Displacement contours are shown for four samples of increasing thickness, approximately 20-, 40-, 60-, and 80-μm. The color bar represents the magnitude of the total 3-D displacement vectors (in micrometers), and the cell has been superimposed on the top surface of the sample. The two edges in the image are included to show that there are negligible displacements detected from neighboring cells (contours are dark blue). Note that the entire gel thickness is not displayed for all samples; instead, only regions of interest are shown. (*B*) Corresponding line plots of the total and individual displacement components taken near the leading edges of the cells. The *x* axis of the plot represents the *z*-position inside the gel with the origin of the *x* axis representing the top surface of the gel.

different region of the matrix forward near its leading edge (Fig. 4*A*). This push–pull aspect of cell migration was detected not only in the in-plane displacements but also in the normal displacement profiles of monitored cells (Fig. 4*B*). The local "pulling" force calculated under the rear portion of the cell shown in Fig. 4*B* (region I, area $\approx 7\ \mu m^2$) is approximately 14 nN, and the total force in the entire region (Fig. 4*B*, region II, area $\approx 16\ \mu m^2$) reaches almost 70 nN. Closer inspection of this profile at a later time reveals a wave-like pattern in the material (Fig. 4 *C* and *D*, Movie S1), indicating a coupling of normal and in-plane displacements.

The push–pull displacement pattern observed within the

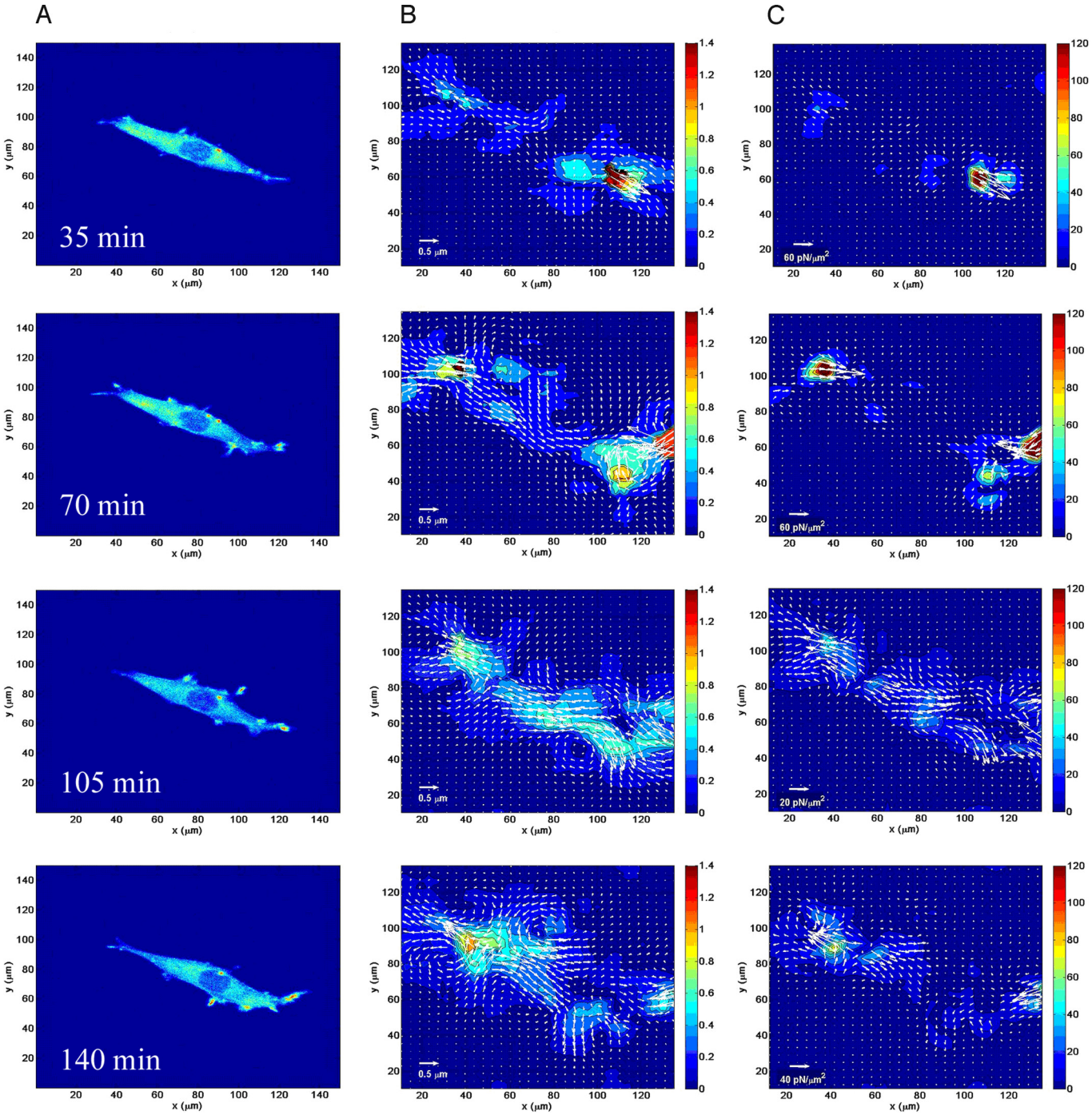

Fig. 3. Time evolution of displacement and traction force contours during cell migration for a single cell. (*A*) A series of four successive confocal images recorded during time-lapse imaging experiment. The images shown were captured every 35 min for a total of 140 min. (*B*) Consecutive displacement contours and vectors resulting from the motile cell shown in Fig. 3*A*. The color bar represents the magnitude of the 3-D displacement vectors, and the arrows represent the in-plane displacement vectors. (*C*) Complementary traction force results calculated directly from displacements in Fig. 3*B*. (Scale bar, 3-D traction forces in pN/μm^2.) Arrows represent the in-plane forces.

material during migration correlates with the extensive polarization and counterbalance of forces that has been shown to occur in cells during locomotion on a 2-D surface (20, 25). This study extends the 2-D analysis of protrusion and retraction forces detected in the surface plane of the material and examines both the pattern and extent to which these counteracting forces penetrate within the 3-D substrate. A distinct advantage of this technique is the ability to analyze force patterns in 3-D, which will allow for the characterization of cell-generated forces in more physiologically relevant microenvironments. Furthermore, by measuring forces in 3-D, it will be possible to directly investigate discrepancies in migration behaviors between 2-D and 3-D models that may be related to force exchange including directional persistence, integrin engagement, and ECM architecture (26). This approach also permits the systematic evaluation of the influence of biophysical and biochemical factors on

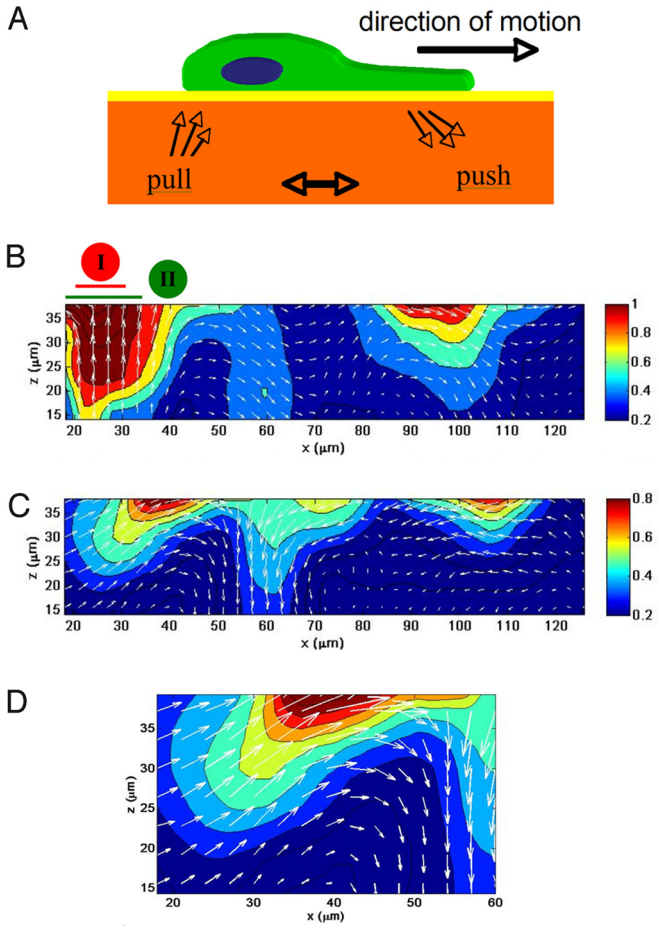

Fig. 4. 3-D push–pull phenomenon observed in the z-plane displacement profiles of tracked cells due to mediated deformation in the gel. (*A*) Schematic of a cell simultaneously pushing and pulling the underlying material during migration. (*B*) The displacement profile in the z-plane illustrates the push–pull hypothesis at t = 35 min. A strong pull upwards near the rear of the cell coordinates with the forward motion of the cell and the pushing of the material near the front of the cell. (*C*) At t = 70 min, the change in the displacement pattern shows the dynamic nature of the 3-D push–pull mechanism, and a magnified view (*D*) shows a more complex pattern that incorporates both normal and in-plane displacements. The color bar represents the magnitude of the total 3-D displacement vectors, and the arrows represent the displacement vectors in the x-z plane.

3-D cell migration and would complement existing force-based computational models for migration in 3-D matrices (27).

Discussion

This report introduces a method to track and quantify cellular traction forces in 3-D by using LSCM and DVC. This combination of techniques allows dynamic interrogation of the complex process of cell migration and yields further insight into the interactions of cells with their extracellular environments. The approach can be used to correlate local force generation with the concentration of focal adhesions during migration and to analyze the interplay of competing force-fields generated by neighboring cells and sheets of cells. Furthermore, the technique can be extended to elucidate changes in traction forces due to malignant transformation, force profiles of encapsulated cells, and the effect of soluble factors on force production.

Materials and Methods

Preparation of Activated Coverslips. Glass coverslips (Gold-Seal coverslip No 0, Electron Microscopy Sciences) were chemically modified to allow covalent attachment of polyacrylamide films using established protocols with some modifications (10, 29). Briefly, coverslips were rinsed with ethanol before being placed in a dish containing a solution of 0.5% (vol/vol) 3-aminopropyltrimethoxysilane (Gelest Inc.) in ethanol for 5 min. The coverslips were removed from the dish and rinsed with a stream of ethanol before being immediately placed treated-side up in a solution of 0.1% (vol/vol) glutaraldehyde (Polysciences, Inc.) in water for 30 min. Activated coverslips were rinsed with a stream of deionized water and left to dry for several hours at 60 °C.

Preparation of Polyacrylamide Films. Thin films of polyacrylamide were generated and fused to functionalized coverslips using a protocol adopted from previous reports with some modifications (10, 29). Solutions of acrylamide (40% wt/vol, Bio-Rad) and N, N-methylene-bis-acrylamide (BIS, 2.5% wt/vol, Bio-Rad) were mixed with distilled water to obtain the following concentrations used for tested samples: (*i*) 10% acrylamide and 0.015% BIS, and (*ii*) 10% acrylamide and 0.0075% BIS. To these solutions, red fluorescent microparticles (0.5 μm, carboxylate-modified, Molecular Probes) were vortexed for 10 s and subsequently added in a volume ratio of 9:100. Cross-linking was initiated through the addition of ammonium persulfate (Sigma–Aldrich) and N, N, N′,N′-tetramethylethylenediamine (Invitrogen). The samples were vortexed for 10 s, and 5–7 μL of the acrylamide solution was pipetted on the surface of a precleaned microscope slide (No. 1, 75 × 25 mm, Corning). To generate thicker films, 20–40 μL of the solution was used. The activated surface of the coverslip was then placed on top of the acrylamide droplet, causing the solution to flatten under the weight of the coverslip. The entire assembly was left undisturbed for 5 min, and then placed in a Petri dish (100-mm diameter, VWR) containing distilled water for 10–30 min. The bonded sample was then peeled from the microscope slide using forceps and thoroughly rinsed with several volume changes of water. Only samples with well-dispersed microparticles were used in the study (> 35 randomly distributed beads per 64 × 64 × 64 voxel subvolume; see examples in ref. 16) as determined by visually inspecting a series of confocal stacks in different regions of the gel sample.

Functionalization of Polyacrylamide Films with Fibronectin. To promote cell attachment to polyacrylamide films, a saturating density of FN was conjugated to the gel surface using the heterobifunctional cross-linker, sulfo-SANPAH (Pierce Chemicals). Adopting procedures outlined in refs. 10 and 29, polyacrylamide gel samples were briefly dried in air to rid the surface of excess water before 200 μL of sulfo-SANPAH in water (1.0 mg/mL) was applied. The surface of the sample was then exposed to unfiltered UV light from a high-pressure mercury lamp (Oriel Q 100W at 5 A, > 10 min warm up time) at a distance of 10 inches for 7.5 min. The darkened sulfo-SANPAH solution was removed from the surface of the gel and replaced with another 200 μL aliquot and irradiated for another 7.5 min for a total of 15 min of UV exposure. The samples were then rinsed vigorously with water for 5 min, and adhered to the bottom of 60 mm Petri dishes (Becton Dickinson) by applying a thin layer of vacuum grease (Dow Corning) around the perimeter of the unmodified side of the coverslip. The samples were rinsed twice with PBS (PBS, pH 7.4), covered with a solution of fibronectin (FN, 0.2 mg/mL, Millipore), and left undisturbed overnight at 4 °C. After overnight incubation, the substrates were rinsed three times with PBS.

Cell Culture. Before depositing cells, FN-modified gel samples were equilibrated in growth media at 37 °C for 15 min. Swiss 3T3 fibroblasts transfected with a GFP-actin vector (a gift from Scott Fraser, California Institute of Technology) were cultured in Dulbecco's Modified Eagle Medium (DMEM) supplemented with 10% FBS, 50 μg/mL streptomycin, and 50 U/mL penicillin (Invitrogen). For all experiments, cells were first treated with Mitotracker Deep Red (Molecular Probes) for 45 min before passaging with trypsin-EDTA (0.05%, Invitrogen). Mitotracker dyes accumulate in actively respiring mitochondria providing an additional method for tracking cells and determining cell viability. Cells were plated at density of approximately 40,000 cells/coverslip, and incubated on samples for 8–12 h before imaging.

Confocal Microscopy and Time-Lapse Imaging. Three-dimensional image stacks were acquired using a Nikon C-1 confocal system mounted on a TE-2000-U inverted optical microscope. A 40× CFI planar fluor air objective with a numerical aperture of 0.6 was used in all experiments. Three laser lines were used to image the cells and the fluorescent microparticles: Argon (488 nm) laser for the GFP-actin, a green HeNe (543 nm) for the microparticles in the polyacrylamide gels, and a red HeNe (633 nm) for the Mitotracker Deep Red for mitochondrial labeling. Confocal stacks were acquired every 35 min for several hours at a resolution of 512 × 512 × H (X × Y × Z) pixels^3, where H ranges from 120 to 250 pixels. In this study, image stacks were acquired every 35 min to minimize phototoxic cell death (significant cell death was observed when time intervals were decreased to 15 and 20 min). Typical imaging areas were approximately

150×150 μm; images with a larger field of view were captured before and after experiments to ensure that measured displacements were not the result of contributions from neighboring cells. A cell was considered ''isolated'' if no other cell could be visualized within 80–100 μm of the selected cell. Visually mitotic cells, as evidence by cell rounding and the formation of two daughter cells, were excluded from analysis. Physiological conditions were maintained during all times by housing the entire confocal microscope inside a custom-built temperature controlled chamber. The temperature was controlled using a feedback-controlled heater, Air-Therm ATX Air Heater Controller (World Precision Instruments), and an arterial blood gas mixture (5% CO_2, 20% O_2, 75% N_2) was injected into the chamber to maintain appropriate culturing conditions.

Calculation of Displacements, Strains, Stresses, and Forces. The full field 3-D displacements are determined using LSCM and DVC, as described in ref. 16. In brief, confocal volume images of cell-seeded polyacrylamide gels with randomly dispersed fluorescent particles are obtained during each time increment. Then, the images are divided into a set of subvolumes that are centered on an area of interest. Using a pair of corresponding subvolume images (e.g., time increment one and two), the local displacement vector can be obtained through a three-dimensional volume correlation method. This is accomplished mathematically by representing the intensity patterns of each subvolume by two intensity functions $f(\mathbf{x})$ and $g(\mathbf{x})$ that have been translated relative to one another by a displacement vector $\mathbf{c}$ in between time increments, i.e., $f(\mathbf{x}) \approx g(\mathbf{x}+\mathbf{c})$. The displacement or translation vector $\mathbf{c}$ of each subset within the confocal volume image can be calculated through the cross-correlation of the two subset intensity functions. The complete mathematical details can be found in a published report (16).

Dividing the entire 3-D confocal volume stack into subsets as described above generates a spatial DVC grid with the gridpoints representing the center or center-displacements of each subset. While this division is adjustable with a maximum division or grid spacing of 1 pixel yielding the highest resolution, it increases the number of necessary computation steps 8-fold per division. To achieve a tractable computation time (≈24–48 h data processing time per experiment), this study used a spatial grid spacing of approximately 2 μm. However, finer (submicrometer) spatial resolution can be selected at greater computational cost.

While the translation-based DVC as briefly outlined above provides accurate results for small strains (<5%), the algorithm presented here has been previously modified to compute large deformations. This has been implemented through the addition of stretch components of the gradient deformation tensor, and has been validated by comparing uniaxial compression data of a hydrogel to theoretical results (16). Although the cell deformations of this study have been shown to be within the small strain approximation, the method is also capable of capturing larger deformations.

Once the entire displacement field ($\mathbf{u}$) is determined, the strain tensor ε of the material substrate is computed using a published displacement-gradient technique (16). Because the material strains measured in this report were found to be <5%, the strain tensor can be expressed as $\varepsilon = (\nabla\mathbf{u}+\nabla\mathbf{u}^{\mathrm{T}})/2$. The material stress tensor σ is then determined through the materials constitutive relations, which were determined from the mechanical characterization results detailed in the *SI Text* describing the material as a linearly elastic, isotropic, incompressible material. Hence, σ is calculated as $\sigma = 2\mu\varepsilon$, where ε is the computed strain tensor as described above and μ is the shear modulus, which is related to elastic (Young) modulus by $E = 2\mu(1 + \nu)$, with $\nu = 0.5$ (incompressible).

Complex material models can be substituted for more complicated substrate materials for computing the stress tensor in future studies, as needed. Finally, traction forces are calculated along the top surface plane, directly beneath the cell using the known Cauchy relationship: $\mathbf{T} = \sigma\mathbf{n}$, where $\mathbf{T}$ is the 3-D surface traction vector, σ is the material stress tensor, and $\mathbf{n}$ is the surface normal.

To establish the maximum resolution of the DVC-LSCM technique for the presented results here, several sets of confocal images of FN-modified polyacrylamide substrate samples were obtained under zero-load conditions (no cells) and physiological conditions every 35 min for approximately 8 h. The computed uncertainties in the displacement measurements were found to be close to the published uncertainties in ref. 16, establishing subpixel or submicrometer resolution. Because the thermal drift of the gel system was found to be negligible and within the limits of the technique, no mathematical manipulation was used to correct the acquired data.

Traction Force Inhibition Using Blebbistatin. Time-lapse imaging of fibroblasts treated with the myosin-II specific blocker, blebbistatin (Sigma–Aldrich), were performed to establish that measured displacements were indeed cell-mediated and not the result of thermal fluctuations within the polyacrylamide sample. Confocal stacks of individual cells were captured 1–2 h before treatment with 12.5 μM blebbistatin, and up to 4 h posttreatment.

ACKNOWLEDGMENTS. We thank Petros Arakelian for help in constructing the experimental setup and Professor Scott Fraser's laboratory for providing the GFP-transfected fibroblasts. This work was funded by a grant from the National Science Foundation through the Center for the Science and Engineering of Materials at the California Institute of Technology. S.A.M. acknowledges support from the National Institutes of Health through a predoctoral National Research Service Award fellowship.

1. Discher DE, Janmey P, Wang YL (2005) Tissue cells feel and respond to the stiffness of their substrate. *Science* 310:1139–1143.
2. Engler AJ, Sen S, Sweeney HL, Discher DE (2006) Matrix elasticity directs stem cell lineage specification. *Cell* 126:677–689.
3. Zaari N, Rajagopalan P, Kim SK, Engler AJ, Wong JY (2004) Photopolymerization in microfluidic gradient generators: Microscale control of substrate compliance to manipulate cell response. *Adv Mater* 16:2133–2137.
4. Pelham RJ, Wang YL (1997) Cell locomotion and focal adhesions are regulated by substrate flexibility. *Proc Natl Acad Sci USA* 94:13661–13665.
5. Ingber DE (2003) Mechanobiology and diseases of mechanotransduction. *Ann Med* 35:564–577.
6. von Wichert G, Sheetz MP (2005) Mechanisms of disease: The biophysical interpretation of the ECM affects physiological and pathophysiological cellular behavior. *Z Gastroenterol* 43:1329–1336.
7. Koo LY, Irvine DJ, Mayes AM, Lauffenburger DA, Griffith LG (2002) Co-regulation of cell adhesion by nanoscale RGD organization and mechanical stimulus. *J Cell Sci* 115:1423–1433.
8. Maskarinec SA, Tirrell DA (2005) Protein engineering approaches to biomaterials design. *Curr Opin Biotechnol* 16:422–426.
9. Wang JHC, Lin JS (2007) Cell traction force and measurement methods. *Biomech Model Mechanobiol* 6:361–371.
10. Dembo M, Wang YL (1999) Stresses at the cell-to-substrate interface during locomotion of fibroblasts. *Biophys J* 76:2307–2316.
11. Roy P, Rajfur Z, Pomorski P, Jacobson K (2002) Microscope-based techniques to study cell adhesion and migration. *Nat Cell Biol* 4:E91–E96.
12. Tan JL, et al. (2003) Cells lying on a bed of microneedles: An approach to isolate mechanical force. *Proc Natl Acad Sci USA* 100:1484–1489.
13. Galbraith CG, Yamada KM, Sheetz MP (2002) The relationship between force and focal complex development. *J Cell Biol* 159:695–705.
14. Harris AK, Wild P, Stopak D (1980) Silicone-rubber substrata - New wrinkle in the study of cell locomotion. *Science* 208:177–179.
15. Balaban NQ, et al. (2001) Force and focal adhesion assembly: A close relationship studied using elastic micropatterned substrates. *Nat Cell Biol* 3:466–472.
16. Franck C, Hong S, Maskarinec SA, Tirrell DA, Ravichandran G (2007) Three-dimensional full-field measurements of large deformations in soft materials using confocal microscopy and digital volume correlation. *Exp Mech* 47:427–438.
17. Lombardi ML, Knecht DA, Dembo M, Lee J (2007) Traction force microscopy in Dictyostelium reveals distinct roles for myosin II motor and actin-crosslinking activity in polarized cell movement. *J Cell Sci* 120:1624–1634.
18. Stephens DJ, Allan VJ (2003) Light microscopy techniques for live cell imaging. *Science* 300:82–86.
19. Levental I, Georges PC, Janmey PA (2007) Soft biological materials and their impact on cell function. *Soft Matter* 3:299–306.
20. Ridley AJ, et al. (2003) Cell migration: Integrating signals from front to back. *Science* 302:1704–1709.
21. Palecek SP, Huttenlocher A, Horwitz AF, Lauffenburger DA (1998) Physical and biochemical regulation of integrin release during rear detachment of migrating cells. *J Cell Sci* 111:929–940.
22. Cox EA, Huttenlocher A (1998) Regulation of integrin-mediated adhesion during cell migration. *Microsc Res Tech* 43:412–419.
23. Vogel V, Sheetz MP (2006) Local force and geometry sensing regulate cell functions. *Nat Rev Mol Cell Biol* 7:265–275.
24. Kovacs M, Toth J, Hetenyi C, Malnasi-Csizmadia A, Sellers JR (2004) Mechanism of blebbistatin inhibition of myosin II. *J Biol Chem* 279:35557–35563.
25. Vicente-Manzanares M, Webb DJ, Horwitz AR (2005) Cell migration at a glance. *J Cell Sci* 118:4917–4919.
26. Even-Ram S, Yamada KM (2005) Cell migration in 3D matrix. *Curr Opin Cell Biol* 17:524–532.
27. Zaman MH, et al. (2006) Migration of tumor cells in 3D matrices is governed by matrix stiffness along with cell-matrix adhesion and proteolysis. *Proc Natl Acad Sci USA* 103:10889–10894.
28. Tian Y, et al. (2006) Adhesion and friction in gecko toe attachment and detachment. *Proc Natl Acad Sci USA* 103:19320–19325.
29. Sabass B, Gardel ML, Waterman CM, Schwarz US (2008) High resolution traction force microscopy based on experimental and computational advances. *Biophys J* 94:207–220.